

CloudDiff: Super-resolution ensemble retrieval of cloud properties for all day using the generative diffusion model

Haixia Xiao^{a,b}, Feng Zhang^{a,*}, Lingxiao Wang^c, Wenwen Li^a, Bin Guo^a, Jun Li^d

^a*CMA-FDU Joint Laboratory of Marine Meteorology, Department of Atmospheric and Oceanic Sciences · Institutes of Atmospheric Sciences, Fudan University, Shanghai, 200438, China*

^b*Key Laboratory of Transportation Meteorology of China Meteorological Administration, Nanjing Joint Institute for Atmospheric Sciences, Nanjing, 210041, China*

^c*RIKEN Interdisciplinary Theoretical and Mathematical Sciences (iTHEMS), Wako, Saitama, 351-0198, Japan*

^d*National Satellite Meteorological Center, China Meteorological Administration, Beijing, 100081, China*

Abstract

Clouds play a crucial role in the Earth's water and energy cycles, underscoring the importance of high spatiotemporal resolution data on cloud phase and properties for accurate numerical modeling and weather prediction. Currently, Moderate Resolution Imaging Spectroradiometer (MODIS) provides cloud products with a spatial resolution of 1 km. However, these products suffer from a lengthy revisit cycle. This study develops a generative diffusion model (donated as CloudDiff) for super-resolution retrieval of high spatiotemporal cloud phase and properties, applicable both day and night. Leveraging 2 km spatial resolution Himawari-8 Advanced Himawari Imager (AHI) thermal infrared (TIR) radiances and viewing geometry as condition, alongside daytime MODIS products as targets, the model can generate cloud phase (CLP), cloud top height (CTH), cloud optical thickness (COT), and cloud effective radius (CER) at 1 km spatial resolution and 10-minute temporal resolution. The conditional diffusion model can generate sharper images and capture finer local features than deterministic super-resolution approaches. It draws multiple samples based on the underlying probability distribution, enabling retrieval uncertainty assessment. Evaluations show agreement between cloud phase and properties derived from the CloudDiff and MODIS cloud products. The ensemble mean is found to enhance retrieval accuracy and credibility, outperforming the deterministic model.

Keywords: Super-resolution, Diffusion model, Cloud properties, Cloud phase, Retrieval

*Corresponding author

Email address: fengzhang@fudan.edu.cn (Feng Zhang)

1. Introduction

Clouds are critical in the Earth’s water and energy budgets (Li et al., 2005). Their influence on the radiation budget can induce either heating or cooling of the planet, contingent upon the radiative characteristics of the cloud and its altitude (Stephens et al., 1981, 1990). The significance of clouds is further underscored by variables such as cloud optical thickness (COT), cloud effective radius (CER), cloud top height (CTH), and cloud phase (CLP). These parameters profoundly impact the Earth’s net radiation balance due to their distinct scattering and absorption characteristics (Fauchez et al., 2018a; Min et al., 2020; Wang et al., 2016a). Achieving an accurate representation of these optical properties remains a formidable challenge, primarily because the microscale physical processes within clouds are difficult to explicitly simulate in global numerical models (Baran, 2012; Ceppi et al., 2017; Waliser et al., 2009). Consequently, there is an urgent need to obtain cloud phase and properties with high spatial and temporal resolution. Such detailed cloud data are indispensable for a deeper understanding of atmospheric physical processes, the enhancement of data assimilation techniques, and the improvement of weather forecasting accuracy (Muskatel et al., 2021).

The retrieval of cloud properties has been conducted for several decades. Since the 1970s, airborne measurements have been employed to retrieve COT and CER, resulting in numerous successful experimental studies (Finger et al., 2015; King, 1987; Krisna et al., 2018; Platnick et al., 1995; Twomey and Cocks, 1989). However, these campaigns incur high costs, and the temporal and spatial coverage of field observations is limited. With the advancement of satellite remote sensing technology, particularly passive sensors (geostationary and polar-orbiting satellites), researchers have increasingly utilized data from visible and near-infrared bands to retrieve cloud properties. This approach enables the characterization of cloud properties at various spatial and temporal resolutions (King et al., 1992; Menzel et al., 2008; Platnick et al., 2003; Tang et al., 2017; Zhang and Platnick, 2011; Zhuge et al., 2020), owing to the wide observational coverage provided by passive sensors. The basic physical principle behind this method is that the cloud radiances measured by the nonabsorptive channels in the visible or near-infrared wavelengths are influenced by COT, while those captured by water-absorption channels in the shortwave infrared wavelength are sensitive to the CER (Nauss and Kokhanovsky, 2011). These retrieval methods, which rely on solar radiation, are effective only for daytime scenes. However, they are not applicable to nighttime scenes and exhibit higher uncertainties in high-latitude regions and optically thin cloud scenes (Wang et al., 2016b).

Thermal Infrared (TIR) retrieval algorithm, utilizing the split-window technique (Parol et al., 1991; Toshiro, 1985), offer valuable capabilities for both daytime and nighttime scene analysis. This technique retrieves COT and CER from the brightness temperature differences between two distinct channels in the infrared atmospheric windows, where gaseous absorption is minimal. Additionally, the optimal estimation methodology (Rodgers, 2000) has been implemented for the Atmospheric Infrared

Sounder V6 (AIRS) and Advanced Microwave Sounding Unit (AMSU), utilizing infrared spectral data to successfully retrieve the physical and optical properties of clouds (Kahn et al., 2014, 2015). However, due to significant absorption by cloud particles in the infrared spectrum, these traditional IR-based algorithms primarily excel in retrieving optically thin cloud properties, while facing challenges in scenarios involving opaque, thick clouds (Wang et al., 2016a). Consequently, an alternative approach is necessary to provide a more comprehensive solution.

The data-driven deep learning method, renowned for their proficiency in capturing the spatial variations of image features with fast computation, have been extensively applied in the cloud identification and properties retrieval (Tong et al., 2023; Zhao et al., 2023). For example, Wang et al. (2022) developed a convolutional neural network (CNN) model for the continuous cloud identification and retrieval of cloud properties (i.e., COT, CER, and CTH) throughout the diurnal cycle for the Moderate Resolution Imaging Spectroradiometer (MODIS), leveraging utilizing daytime MODIS TIR radiances alongside satellite viewing zenith angles (VZA). Additionally, employing a transfer-learning-based UNet model and MODIS/Himawari-8 cloud products, Li et al. (2023) successfully estimated the CER, COT, and CTH from Himawari-8 TIR measurements, and results showed that the model enhanced performance for optically thick clouds.

Previous research has relied on either polar-orbiting (e.g., MODIS) or geostationary (e.g., Himawari-8 Advanced Himawari Imager) satellite sensors for cloud property estimation. While polar-orbiting satellites offer high-resolution cloud products (1 km resolution), they suffer from a lengthy revisit cycle, impacting temporal resolution. Conversely, geostationary satellites provide frequent revisits, offering high temporal resolution and continuous cloud observation (Meng et al., 2024). However, their spatial resolution is lower compared to polar-orbiting satellites. Hence, combining data from both types of satellites to achieve high spatiotemporal resolution in cloud phase and properties is a promising direction to explore.

For high-impact weather events such as severe convective storms, tropical and extratropical cyclones, the underlying dynamical and thermodynamic mechanisms are complex, leading to significant uncertainties in retrieving their cloud properties. Unfortunately, current CNN/UNet retrieval methods primarily focus on deterministic modeling, which often neglects the inherent uncertainties within the data. Diffusion models, a novel category of likelihood-based models recently highlighted for generating high-quality images (Sohl-Dickstein et al., 2015; Song and Ermon, 2019), offer desirable characteristics such as distribution coverage (Ho et al., 2020). Unlike deterministic retrieval methods, diffusion models derive probability distribution functions and can generate a large number of samples (Ho et al., 2020; Ling et al., 2024; Bishop, 2024), while guaranteeing that the retrieval distribution encapsulates all plausible outcomes, thus allowing for estimating the probability density and its score. Diffusion models have proven successful in various research domains, such as computer vision for image generation and synthesis (Croitoru, 2023), precipitation nowcasting (Nai

et al., 2024), estimating the unresolved geophysical processes (Pan et al., 2023), and earth system model downscaling (Hess et al., 2024), showcasing their effectiveness in handling complex systems.

The primary objective of this study is to develop a diffusion model aimed at super-resolution high spatiotemporal resolution cloud optical properties and cloud phase retrieval throughout the diurnal cycle using a geostationary satellite. Leveraging the TIR channels of the Himawari-8 satellite and employing MODIS cloud products as ground truth, we have developed a generative diffusion model capable of cloud identification and retrieval of COT, CER, and CTH, characterized by high precision and enhanced spatiotemporal resolution. The efficacy of this model is evaluated against standard MODIS cloud product measurements, focusing particularly on its generalization capabilities and the uncertainty, analyzed across typhoon case studies and extended datasets. The data, methodology, and experimental details are outlined in Section 2. The performance outcomes of the model are thoroughly examined in Section 3. Lastly, Section 4 offers conclusions and discussions.

2. Data and methods

2.1. Data

2.1.1. Himawari-8 AHI Satellite Data

Himawari-8, launched in October 2014, is the geostationary satellite sensor system operated by the Japan Meteorological Agency (JMA). It represents the latest iteration in the Multifunctional Transport Satellite (MTSAT) series. The Advanced Himawari Imager (AHI) sensor onboard Himawari-8 captures full disk images every 10 minutes across 16 spectral bands from visible to infrared wavelengths, with spatial resolutions ranging from 500 m to 2 km and temporal resolutions between 2.5 and 10 minutes, covering regions from East Asia to Australia. The TIR measurements are sensitive to optically thin clouds and are continuously obtained throughout the diurnal cycle, independent of solar geometry (Fauchez et al., 2018a). In this study, TIR radiations from Himawari-8 AHI are utilized to estimate cloud properties during both daytime and nighttime. Additionally, the VZA are employed to construct the retrieval model. Table 1 summarizes the used TIR measurements (6.95–13.30 μm) and VZA of Himawari-8 AHI.

2.1.2. MODIS data

With the launch of NASA’s Terra satellite in 1999, followed by Aqua in 2002, MODIS has emerged as one of the most indispensable satellite remote sensing platforms for Earth science research. It measures reflected solar and emitted thermal radiation across 36 spectral channels (0.42–14.24 μm), offering unique spectral and spatial capabilities for retrieving cloud properties (Platnick et al., 2016). The Terra-MODIS (MOD06) and Aqua-MODIS (MYD06) products, which have a spatial resolution of 1 km, are accessible through the Atmosphere Archive and Distribution System website

(<https://ladsweb.modaps.eosdis.nasa.gov/>). These products include cloud top properties (e.g., CTH, CLP for both day and night) and cloud optical and micro-physical properties (e.g., COT, CER, daytime only). Over the years, the MODIS cloud products have demonstrated consistent high accuracy and reliable performance (King et al., 2003; Platnick et al., 2015). In this study, the daytime MODIS cloud optical and physical properties (CTH, COT, CER, and CLP) from the Level-2 cloud product (MYD06 L2 and MOD06 L2) are utilized as ground truth to develop the super-resolution retrieval model.

Table 1: The Himawari-8 AHI data used for cloud parameter super-resolution retrieval.

Band Number	Bandwidth (μm)	Central Wavelength (μm)	Spatial resolution (km)	Spatial resolution (minute)
9	6.89–7.01	6.95		
10	7.26–7.43	7.35		
11	8.44–8.76	8.6		
12	9.54–9.72	9.63	2	10
13	10.3–10.6	10.45		
14	11.1–11.3	11.20		
15	12.2–12.5	12.35		
16	13.20–13.40	13.30		
VZA	–	–		

2.1.3. Data preprocessing

As described above, the TIR measurements (6.95 μm , 7.35 μm , 8.60 μm , 9.60 μm , 10.45 μm , 11.20 μm , 12.35 μm , and 13.30 μm) along with the VZA of the Himawari-8 AHI serve as the inputs for the model, while the MODIS level-2 CLP, CTH, COT, and CER data are used as the targets for training the model. To optimize the model during training and enhance its accuracy, we normalized the inputs and targets. By employing min-max normalization, we scaled the input and output variables to fall within the range of 0 to 1.

To cover as wide a range of the Earth’s surface and viewing geometries as possible, and to accommodate seasonal variations, we collected data from January 2016 to October 2017. Specifically, data from January 2016 to May 2017 was utilized for model training, data from June to August 20, 2017 for model validation, and data from August 21, 2017, to October 2017 served as the test set. Owing to the differing spatiotemporal resolutions of the Himawari-8 AHI and MODIS cloud products, we performed spatiotemporal matching of the data. In this process, we selected data from both MODIS and Himawari-8 for the same regions and times, with the cloud product grid points being twice that of the TIR observations. To alleviate memory and computational demands and to accelerate the selection process for the model,

we cropped the cloud products in the training, validation, and test sets to a size of 256×256 km, while the input TIR observations were sized at 128×128 km. Ultimately, our training set comprised 76,247 samples, with the validation and test sets containing 9,530 and 9,532 samples, respectively.

2.2. Method

The diffusion model is a state-of-the-art deep learning technique that employs probabilistic denoising processes to develop generative models (Bishop, 2024). The model typically operates on the principle of simulating a gradual process of denoising, effectively reconstructing data points from a noise-like distribution. This process is modeled as a reverse Markov chain, where a data sample is initially transformed into noise through a sequence of diffusion steps and then reconstructed back into a clean sample through learned reverse transitions. In a classical set-up, the model involves iteratively applying a series of conditional Gaussian distributions, beginning from a distribution of noise $p(\mathbf{z}_T)$ and progressively denoising it to retrieve the original data distribution $p(\mathbf{x}_0)$. This can be succinctly represented as,

$$p(\mathbf{x}_0) = \int \cdots \int p(\mathbf{x}_0|\mathbf{x}_1)p(\mathbf{x}_1|\mathbf{x}_2) \cdots p(\mathbf{x}_{T-1}|\mathbf{z}_T)p(\mathbf{z}_T) d\mathbf{x}_1 \cdots d\mathbf{x}_{T-1}d\mathbf{z}_T. \quad (1)$$

In each iteration, the model utilizes the noisy data from the previous step as input, subsequently refining it to a greater degree of accuracy in accordance with the data’s original state. The denoising path is learned from training data, thereby enabling the model to effectively generate or reconstruct high-quality data samples.

2.2.1. Conditional diffusion model

In our study, these TIR measurements and VZA variable are denoted by \mathbf{y} which is the condition variable. The target variables, cloud products, are represented by \mathbf{x} . The objective is to approximate the conditional distribution of \mathbf{x} given \mathbf{y} , using a significantly large dataset of paired samples $(\mathbf{x}_i, \mathbf{y}_i)$. The conditional diffusion model incorporates conditioning variables into the generative process (Batzolis, 2021), allowing the model to generate data conditioned on specific information. Mathematically, this can be represented as the transition from a noise distribution $p(\mathbf{z}_T)$ to the data distribution $p(\mathbf{x}_0)$ conditioned on a variable \mathbf{y} , described by,

$$p(\mathbf{x}_0|\mathbf{y}) = \int p(\mathbf{x}_0|\mathbf{z}_T, \mathbf{y})p(\mathbf{z}_T|\mathbf{y}) d\mathbf{z}_T, \quad (2)$$

where, \mathbf{z}_T represents the latent variables at the final timestep, and the model iteratively refines these variables through the conditioning on \mathbf{y} , enhancing its ability to target specific data generation tasks. As Figure 1 shows, the conditional diffusion model enables to produce cloud products given the conditions of TIR and VZA variables, making it particularly useful in scenarios where the output needs to be tailored to specific environments. In this framework, for any given \mathbf{y} , the algorithm

outputs samples of \mathbf{x} from $\mathbf{x} \sim p(\mathbf{x}_0|\mathbf{y})$, where p is a learned distribution that does not adhere to any predefined probability distribution form. The forward process has the same scheme as the Denoising Diffusion Probabilistic Models(DDPMs) (Ho et al., 2020), but in the reverse process we embed the conditional variables into the UNet for modelling the conditional probability distributions (Nai et al., 2024).

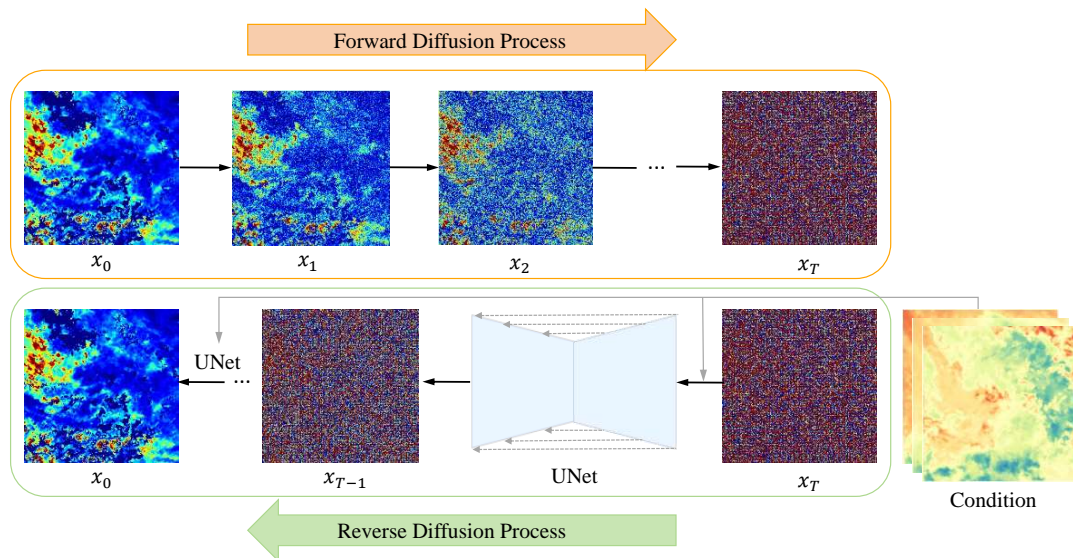


Figure 1: The CloudDiff for super-resolution cloud identification and properties retrieval. The generated samples \mathbf{x} are cloud products, and the conditions \mathbf{y} includes TIR and VZA variables.

In the forward process, the data \mathbf{x}_0 undergoes a series of transformations, gradually adding noise over discrete time steps T until it is converted into pure Gaussian noise $\mathbf{x}_T \equiv \mathbf{z}_T$. The noise addition at each timestep t is defined by a variance schedule β_t , and can be described by the following stochastic differential equation,

$$\mathbf{x}_t = \sqrt{1 - \beta_t} \mathbf{x}_{t-1} + \sqrt{\beta_t} \epsilon, \quad \epsilon \sim \mathcal{N}(0, \mathbf{I}), \quad (3)$$

where ϵ represents Gaussian noise.

The reverse process, where the model learns to reconstruct the original data from noise, is explicitly conditioned on \mathbf{y} . At each step, the model estimates the original data \mathbf{x}_{t-1} from the current noisy data \mathbf{x}_t using a neural network parameterized by $\{\theta\}$. This network predicts the mean $\mu_\theta(\mathbf{x}_t, t, \mathbf{y})$ of the distribution for \mathbf{x}_{t-1} , typically modeled as,

$$\mathbf{x}_{t-1} = \mu_\theta(\mathbf{x}_t, t, \mathbf{y}) + \sigma_t \epsilon, \quad \epsilon \sim \mathcal{N}(0, \mathbf{I}), \quad (4)$$

where σ_t is a predetermined noise level (Ho et al., 2020).

The objective of training this conditional diffusion model is to minimise the difference between the estimated \mathbf{x}_{t-1} and its actual value. This effectively allows the model to learn the reverse of the forward diffusion process. The loss function is originally from the Fisher divergence (Song and Ermon, 2019; Song et al., 2021; Nai et al., 2024), but equivalently used as a variant of the mean squared error between the predicted and actual previous timestep values, conditioned on \mathbf{y} ,

$$\mathcal{L}(\theta) = \mathbb{E}_{\mathbf{x}_0, \epsilon, \mathbf{y}} [\|\epsilon - \epsilon_\theta(\mathbf{x}_t, t, \mathbf{y})\|^2], \quad (5)$$

where ϵ_θ represents the outputs of the UNet as the predictions of the noise used to generate \mathbf{x}_t from \mathbf{x}_{t-1} . To improve the representation ability, we have introduced the multi-head attention modules into the UNet architecture (Vaswani et al., 2017).

After training, the conditional diffusion model (hereafter, CloudDiff) is capable of generating multiple samples simultaneously. In our tests, we generate 30 samples per evaluation instance. These samples are reminiscent of the ensemble members used in numerical weather prediction’s dynamical models, which employ large numbers of members for ensemble predictions (Li et al., 2024). Furthermore, we conduct comparative analyses between the CloudDiff and established deterministic data-driven methods. For this purpose, the study uses a supervised learning approach with a UNet architecture (Trebing et al., 2021), referred to as the deterministic model, as the benchmark. This method is specifically applied to the tasks of super-resolution retrieval of cloud properties and cloud identification, serving as a baseline for performance comparison.

2.2.2. Performance evaluation

The CloudDiff serves as a super-resolution approach that requires an appropriate evaluation scheme. Although intuitive, sample-by-sample comparisons cannot fully demonstrate the effectiveness of the super-resolution technique. To obtain a comprehensive performance evaluation, we collect MODIS labels for assessing the quality of the generated cloud products. Consequently, we employ Mean Absolute Error (MAE) and Mean Squared Error (MSE) as metrics, allowing for a quantitative assessment of the model’s performance in enhancing spatial resolution. These metrics, commonly used in cloud properties retrieval (Wang et al., 2022; Zhao et al., 2023), are defined as follows,

$$\text{MAE} = \frac{1}{NN_p} \sum_{i=1}^N \sum_{j=1}^{N_p} |x_{i,j} - \hat{x}_{i,j}|, \quad (6)$$

$$\text{RMSE} = \sqrt{\frac{1}{NN_p} \sum_{i=1}^N \sum_{j=1}^{N_p} (x_{i,j} - \hat{x}_{i,j})^2}, \quad (7)$$

where N represents the number of samples, x_i denotes the values from MODIS cloud products, and \hat{x}_i represents the super-resolution retrieved cloud products. N_p indicates the number of pixels for each sample, and j labels the index of the pixels. It

should be noted that a more accurate super-resolution model will have a smaller root mean square error (RMSE) and mean absolute error (MAE).

3. Results

3.1. Case study

We begin our study with a case analysis focusing on Typhoon Hato (No.1713) over the offshore areas of China to evaluate the performance of the CloudDiff and comprehend its uncertainty. Typhoon Hato developed in the northwest Pacific Ocean at 06:00 UTC on August 20, 2017, and progressively intensified. By 01:00 UTC on August 23, it had escalated to a severe typhoon, peaking at Category 16 with maximum sustained winds of 52 m/s. It made landfall near Zhuhai City, Guangdong Province, China, around 04:50 UTC on August 23 as a severe typhoon, causing substantial devastation in southern China. On that day, the Terra satellite passed over the coastal Zhuhai area around 02:50 UTC; thus, our analysis primarily focused on evaluating the retrieved COT, CER, CTH, and CLP at this specific time. The analysis covered the typhoon area between 19.78°N – 22.32°N and 111.68°E – 114.22°E , corresponding to a grid size of 256×256 .

Figure 2 presents the various cloud properties generated by the CloudDiff across 30 samples and grid points where MODIS cloud properties were not captured by samples. Since all 30 CLP samples indicated ice clouds within the study area, CLP results are not displayed. It is observed that the cloud properties generated by different samples vary slightly but generally reflect the typhoon’s morphology accurately. Despite variations in COT values among the samples and differing degrees of overestimation and underestimation in the typhoon’s cloud wall, they accurately estimated the optical thickness at the typhoon eye. Notably, underestimation occurred for COT values over 90 at about 16.03% of the grid points, and overestimation at 1.67% of the grid points, while COT values below 60 were well retrieved. Regarding CER, some samples did not accurately represent the CER, generally overestimating (9.68%, mainly around the typhoon eye) and underestimating (12.49%, mainly in the typhoon’s cloud wall). Additionally, samples underestimated CTH to various extents, particularly on the west and southwest sides of the typhoon eye, with a total underestimation of 30.41% in CTH and a mere 0.63% overestimation.

To evaluate the performance and uncertainty of the CloudDiff, we compared the cloud properties with those from the deterministic model (Fig. 3). The results show that individual sample produces more sharpness and more local details of COT, CER, and CTH compared to the ensemble mean (appears blurrier). The deterministic model’s results blurrier than the ensemble mean and also lack detail. Regarding COT, compared to MODIS cloud products, the sample underestimated the COT in the typhoon eye region and overestimated areas with $\text{COT} < 90$. The ensemble mean (the mean values of 30 samples) also overestimated the extent of $\text{COT} < 90$ but reported lower values than single sample, somewhat correcting the underestimation of COT in

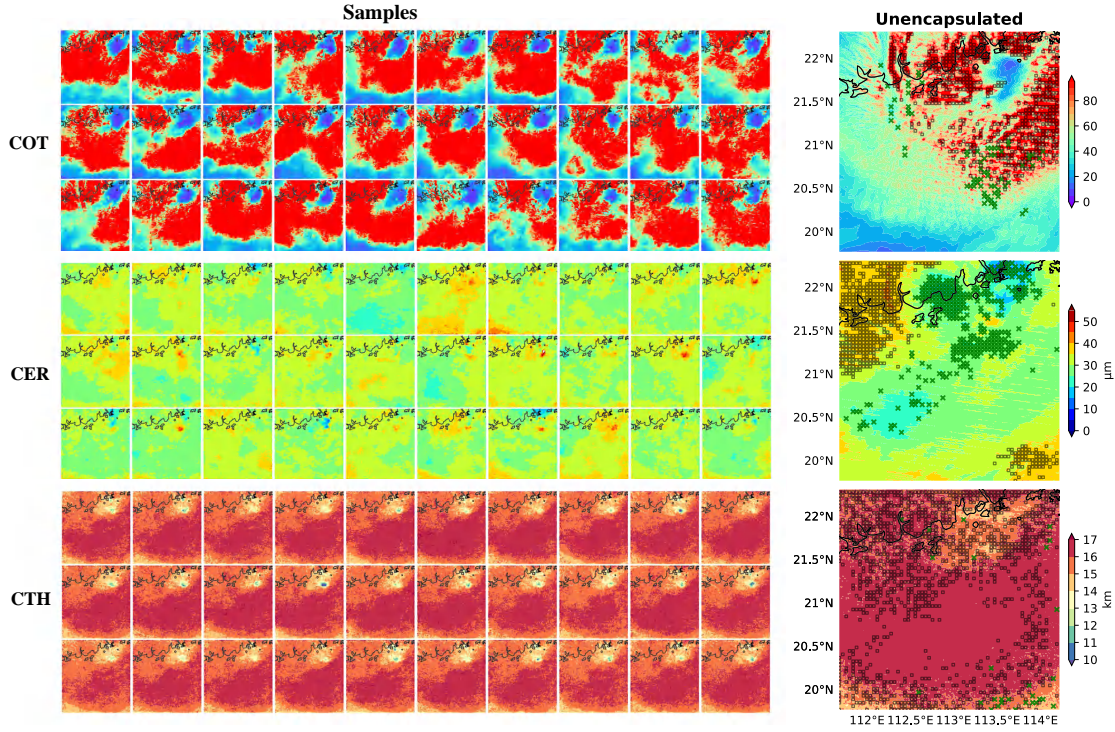


Figure 2: Cloud properties retrieval in the typhoon Hato region centering around 21.8°N, 113.8°E at 0250 UTC on August 23, 2017, was conducted using the CloudDiff. The columns represent samples and grid points where MODIS cloud properties are not captured by samples. The underestimation and overestimation are respectively indicated by black squares and green 'x'. The background is colored based on MOD06 cloud products.

the typhoon eye region by single sample. The standard deviation of 30 samples, which can donate the retrieval uncertainty, indicates large error in the estimates of COT in the typhoon's cloud wall, mainly because most samples overestimated the COT in this area (see Fig. 2). The deterministic model not only overestimated the extent of COT >90 (with lower internal values) but also underestimated the optical thickness on the western side of the typhoon eye. Both single sample and ensemble mean, as well as the deterministic model, inaccurately retrieved areas with CER >35 μm and overestimated the CER in the typhoon eye area. However, the CloudDiff exhibited smaller biases in CER retrievals compared to the deterministic model, and standard deviations mostly below 6 μm across most regions, indicating small uncertainty.

Regarding CTH, CloudDiff exhibits minimal uncertainty, with standard deviations generally below 1 km across most regions. compared to MODIS, the ensemble mean more accurately represented CTH in the southern part of the typhoon eye than individual samples, but it underestimated areas with CTH greater than 16 km and the CTH in the typhoon eye. The deterministic model also underestimated CTH greater than 16 km and the CTH in the typhoon eye. Additionally, deterministic model

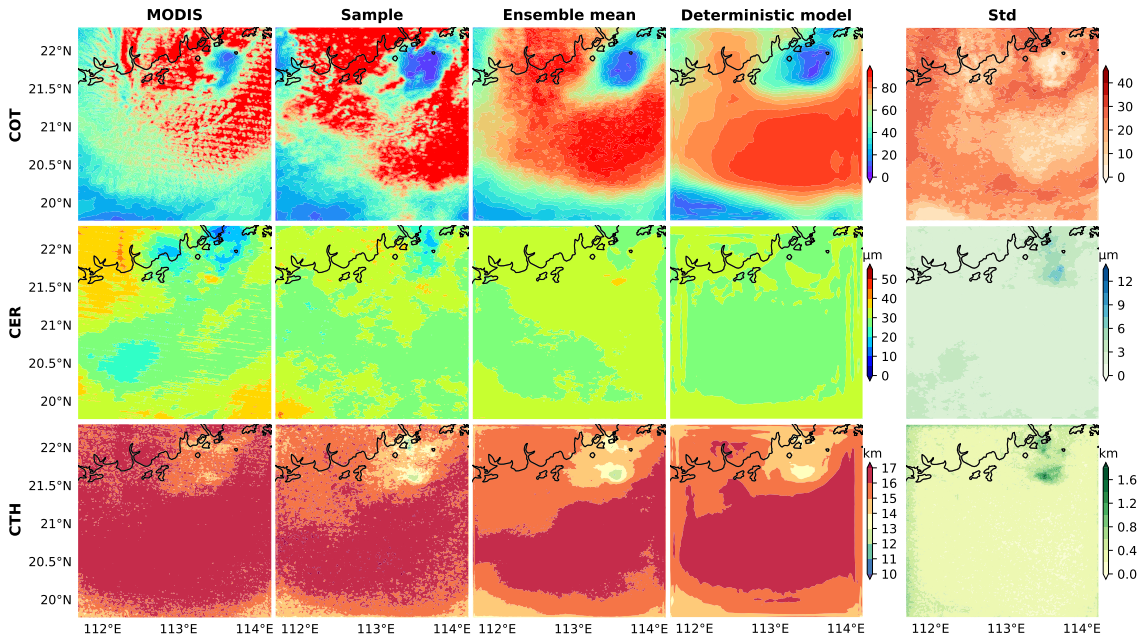


Figure 3: MOD06 cloud products and retrieved cloud properties in the typhoon Hato region at 0250 UTC on August 23,2017. The columns are MOD06 cloud products, sample, esemble means, deterministic model, and standard deviation (std).

underestimated CTH at the image edges. Moreover, both the ensemble mean and deterministic model accurately retrieved CLP (not showed), consistent with MODIS cloud classification results. Overall, the super-resolution cloud properties retrieval based on the CloudDiff proved superior to those from the deterministic model, providing sharper and more localized details of 1 km cloud properties during the typhoon event.

Using 30 samples generated by the CloudDiff, we computed probability estimates for various thresholds of cloud property estimates and cloud phase probability results (Fig. 4), which deterministic model cannot provide. Based on the thresholds provided by the International Satellite Cloud Climatology Project (ISCCP) for COT and CTH associated with cloud types, we computed probability estimates for COT (Fig.4b,c,d) and CTH (Fig.4j,k,l) at similar thresholds in ISCCP. The results indicate that the probability estimates from the CloudDiff are close to with MODIS data, with probabilities exceeding 80% in the $3.6 < COT < 23$ and $23 < COT$ regions. Additionally, all MODIS CTH values were greater than 6.4 km, and the CloudDiff estimated probabilities of $CTH > 6.4$ km to be over 90%.

Following ISCCP cloud classifications, the predominant cloud types in the typhoon eye and its southwestern sea regions are cirrostratus, while other areas feature deep convection clouds. For CER, thresholds of $20 \mu\text{m}$ and $40 \mu\text{m}$ were selected for probability estimation (Fig.4f,g,h), revealing that the CloudDiff's CER estimates primarily

fall within the $(20, 40]$ range, with very low probabilities for CER in the $(0, 20]$ and $\text{CER} > 40 \mu\text{m}$ ranges. In comparison to MODIS, the CloudDiff tends to overestimate CER in the typhoon eye and underestimate CER over the western land areas of the typhoon eye. Furthermore, the CloudDiff’s probability estimates for clouds classified as ice clouds in the study area exceed 99 % (not showed) , aligning well with MODIS. Overall, through probabilistic estimation, we can better ascertain the range of cloud property values and cloud phase, evaluate the uncertainty in cloud property retrieval and identification, and enhance the accuracy of super-resolution retrievals.

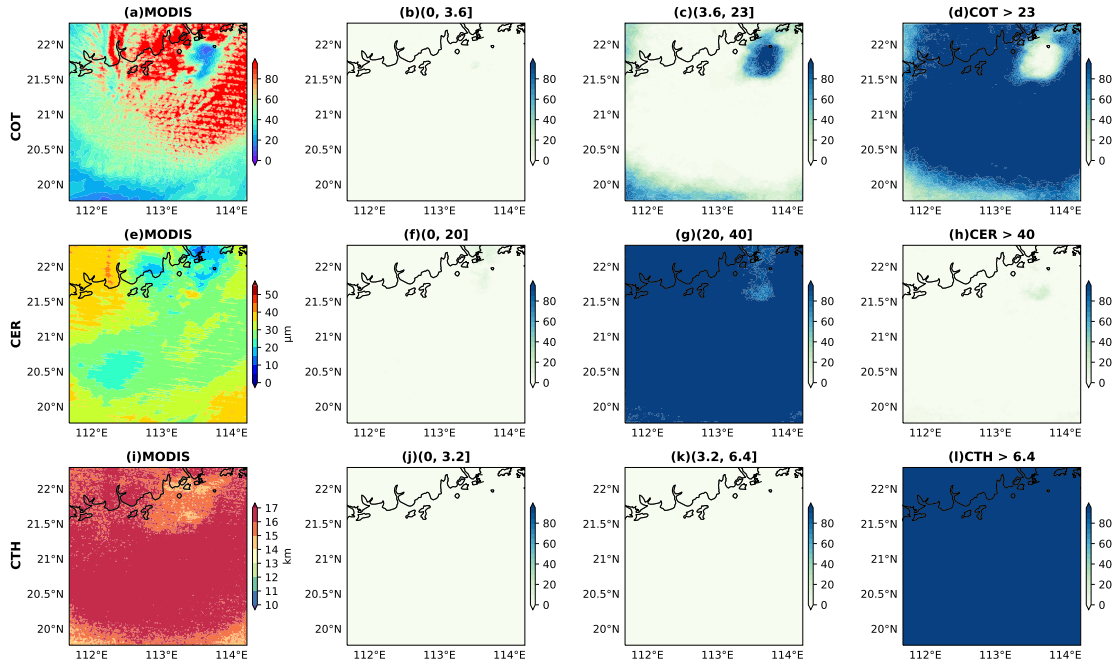


Figure 4: The probability estimates for cloud properties in the typhoon Hato region at 0250 UTC on August 23,2017. (b-d) present the probability estimates of COT within different threshold ranges.(f-h) display the probability estimates of CER for varying thresholds. (j-l) show the probability estimates for CTH across different threshold ranges.

3.2. Overall evaluation

We evaluated the overall performances of the models using data from the test set. We employed MSE and RMSE metrics to evaluate cloud properties. A comparative analysis was conducted to investigate how the number of samples affects the super-resolution retrieval performance. This analysis included ensemble means with 1 and 30 samples. Additionally, we compared these results with those from the deterministic model. Figure 5 illustrates the RMSE and MSE comparisons between the MODIS cloud products and the super-resolution retrieval results.

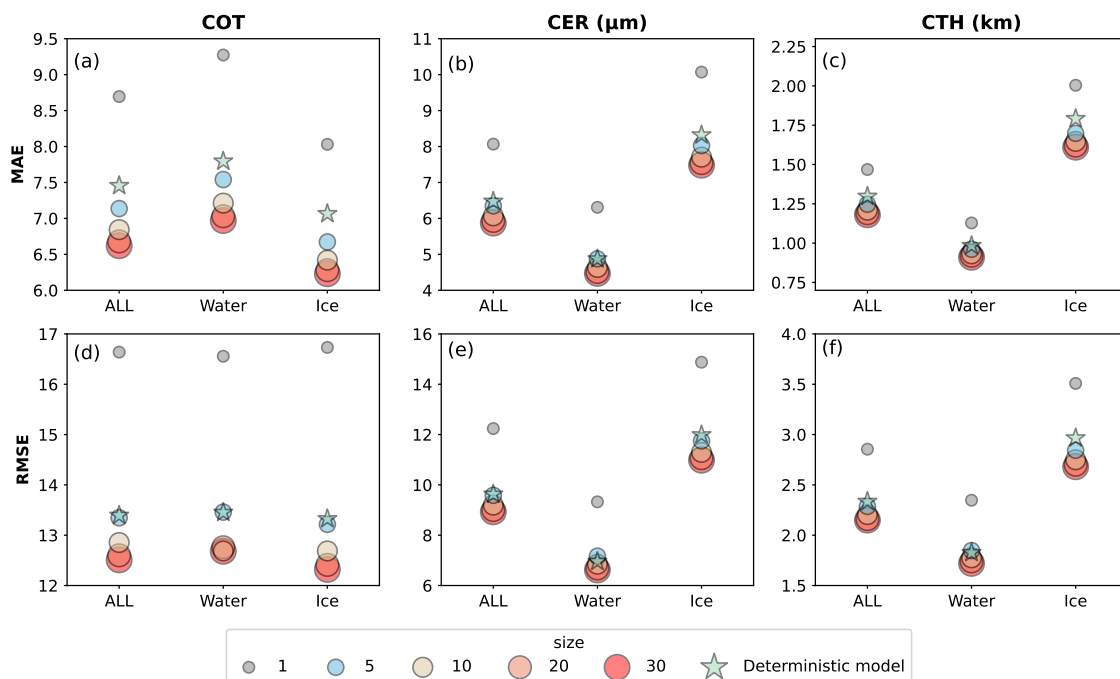


Figure 5: The performance evaluation of cloud properties. Skill metrics were calculated between the CloudDiff/deterministic model and MODIS cloud products. Different sizes of circles represent ensemble sizes ranging from 1 to 30, while pentagrams indicate deterministic model.

For COT, CER, and CTH, the results indicate significantly higher MAE and RMSE values when the ensemble size is 1. As the ensemble size increases beyond five, both the MAE and RMSE of the ensemble mean gradually decrease. An interesting observation is that the improvement in super-resolution retrieval capability from 20 to 30 samples is relatively minor, suggesting that approximately 20 samples are sufficient to capture most of the high-resolution details and adequately cover the uncertainty space in the retrieval process. The MAE and RMSE values of the deterministic model retrieval approach those when the ensemble size is 5, and are notably lower than those observed with an ensemble size of 30.

Specifically, for COT at an ensemble size of 30, the ensemble mean MAE for all clouds (water and ice) is 6.62, with an RMSE of 12.51, compared to the deterministic model results which have an MAE of 7.45 and an RMSE of 13.48. For water clouds alone, the MAE is 6.97 and the RMSE is 12.68, with ice clouds showing slightly better performance (MAE = 6.23, RMSE = 12.32). For CER, the ensemble mean MAE for all clouds at an ensemble size of 30 is $5.87\mu\text{m}$, with an RMSE of $8.93\mu\text{m}$. Water clouds exhibit a lower MAE of $4.47\mu\text{m}$ and RMSE of $6.62\mu\text{m}$, whereas ice clouds have a higher MAE of $7.48\mu\text{m}$ and RMSE of $10.98\mu\text{m}$. Similarly, for CTH at the same ensemble size, the ensemble mean MAE for all clouds is 1.18 km, with an RMSE of 2.15 km. The MAE for water clouds is 0.91 km and RMSE is 1.72 km, with ice clouds performing worse (MAE = 1.61 km, RMSE = 2.68 km).

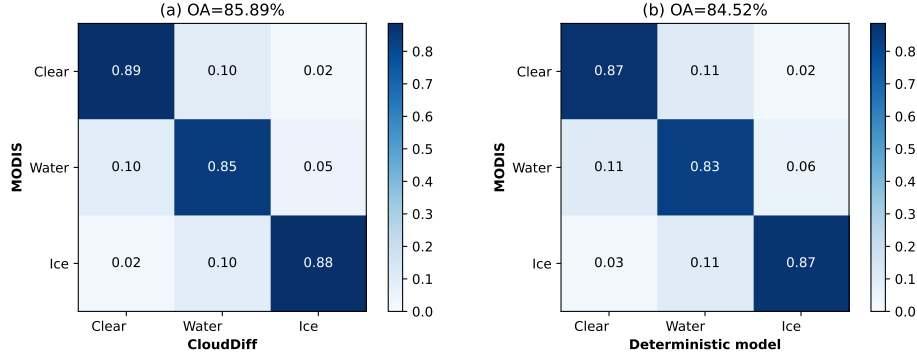


Figure 6: Confusion matrix of CLP products between MODIS and CloudDiff (a), deterministic model (b). 'OA' is the overall accuracy

In addition, the cloud identification results were assessed. Here, we primarily compared the performance of the deterministic model with the ensemble mean results of 30 samples. The validation results demonstrate the model's capability to accurately identify true targets from MODIS data. Figure 6 presents the CLP identification results for the ensemble mean of the CloudDiff (Fig. 6a) and the deterministic model (Fig. 6b), which categorize the targets primarily into clear sky, water clouds, and ice clouds. The CloudDiff achieves an overall accuracy (OA) of 85.89%. Specifically, it shows a retrieval accuracy for clear sky and ice clouds of 89% and 88% respectively, and 85% for water clouds. In contrast, the deterministic model exhibits a retrieval accuracy of 88% for both clear sky and water clouds, but a slightly lower accuracy of 83% for ice clouds, with an OA of 84.52%, which is marginally lower than that of the CloudDiff. Overall, the ensemble mean of the CloudDiff demonstrates superior performance in identifying clear sky, water clouds, and ice clouds compared to the deterministic model.

In summary, the CloudDiff enables the efficient generation of realistic samples that are faithful to a broad range of resolved retrieval schemes and sufficiently diverse to cover most plausible outcomes.

4. Conclusions

In this study, we propose a conditional diffusion model named CloudDiff for cloud identification and retrieval of COT, CER, and CTH. The model is trained on 2 km TIR measurements from AHI onboard the Himawari-8 and satellite VZA, using MODIS 1 km resolution cloud products as training data. This CloudDiff is capable of generating cloud properties and CLP with high spatiotemporal resolution (1 km, 10-minute). It can produce various samples to effectively cover the distribution and range of cloud properties and also offers uncertainty estimates.

Evaluation of the model on Typhoon Hato demonstrates that the 30 samples generated by the CloudDiff accurately capture the range of COT, CER, and CTH during

the typhoon event and effectively identify cloud phases. Compared to the deterministic model, the CloudDiff’s cloud properties more closely align with MODIS cloud products and improve the sharpness of the super-resolution retrieval. Additionally, the model can provide probability estimates for different threshold cloud properties, significantly enhancing retrieval accuracy. Further evaluation on the test set shows that MAE and RMSE decrease as the ensemble size increases, with the lowest errors observed at an ensemble size of 30. The performance of deterministic model matches that of the ensemble mean when the ensemble size is 5, underscoring the superior results of the CloudDiff. The results clearly demonstrate that increasing the samples size enhances retrieval capabilities, but this improvement is minimal beyond a certain size; for instance, increasing the ensemble size from 20 to 30 offers little improvement.

Although the CloudDiff has shown promising results, further improvements are still possible. Integrating additional conditional variables such as ERA5 meteorological data could improve the super-resolution retrieval effectiveness. Given adequate computing resources, it is feasible to generate more samples and determine the optimal ensemble size for even better performance. Future work will involve case studies of high-impact weather events to further assess the CloudDiff’s performance and explore specific applications in ensemble retrieval.

We hope that the demonstrated utility of generative artificial intelligence technology for cloud identification and probabilistic retrieval will promote its application in remote sensing, which is crucial for quantifying uncertainty in identification and forecasting weather events such as typhoons. We believe it is time to explore the potential of diffusion models in cloud remote sensing, offering a promising solution for challenges such as cloud image forecasting and satellite precipitation estimation.

Declaration of Competing Interest

The authors declare that they have no known competing financial interests or personal relationships that could have appeared to influence the work reported in this paper.

Acknowledgments

This work was supported by the National Natural Science Foundation of China (42222506 and 42075125). L. Wang also thanks the National Natural Science Foundation of China (12147101) for supporting his visit to Fudan University. The authors would like to thank NASA for freely providing the Himawari-8 products (<https://www.eorc.jaxa.jp/ptree/index.html>) and MODIS data online (<https://ladsweb.modaps.eosdis.nasa.gov/>). We acknowledge Xiaoye Wang from Fudan University for assisting with data processing.

References

- Baran A.J., *From the single-scattering properties of ice crystals to climate prediction: A way forward*, Atmospheric Research, 112, pp. 45-69, 2012.
- Batzolis, G., Stanczuk, J., Schönlieb, C. B., and Etmann, C., *Conditional image generation with score-based diffusion models*, in arXiv, arXiv:2111.13606.
- Bishop, C.M., Bishop, H., *Deep Learning: Foundations and Concepts*, Springer International Publishing, Cham, Switzerland, 2024.
- Croitoru, Florinel-Alin and Hondru, Vlad and Ionescu, Radu Tudor and Shah, Mubarak, *Diffusion Models in Vision: A Survey*, in IEEE Transactions on Pattern Analysis and Machine Intelligence, vol. 45, no. 9, pp. 10850-10869, 1 Sept. 2023.
- Ceppi P., Briant F., Zelinka M.D., Hartmann D.L., *Cloud feedback mechanisms and their representation in global climate models*, Wiley Interdisciplinary Reviews: Climate Change, 8(4), e465, 2017.
- Fauchez, T., Platnick, S., Sourdeval, O., et al., *Cirrus Horizontal Heterogeneity and 3-D Radiative Effects on Cloud Optical Property Retrievals From MODIS Near to Thermal Infrared Channels as a Function of Spatial Resolution*, Journal of Geophysical Research: Atmospheres, 123(19), pp. 11,141-11,153, 2018.
- Finger, F., Werner, F., Klingebiel, M., et al., *Spectral optical layer properties of cirrus from collocated airborne measurements and simulations*, Atmospheric Chemistry and Physics, 16(12), pp. 7681-7693, 2015.
- Hess P., Aich M., Pan B., & Boers N., *Fast, Scale-Adaptive, and Uncertainty-Aware Downscaling of Earth System Model Fields with Generative Foundation Models*, 2024, arXiv preprint arXiv:2403.02774.
- Ho J., Jain A., Abbeel P., *Denoising diffusion probabilistic models*, Advances in Neural Information Processing Systems, 33, pp. 6840-6851, 2020.
- Kahn B.H. et al., *The Atmospheric Infrared Sounder version 6 cloud products*, Atmospheric Chemistry and Physics, 14(1), pp. 399-426, 2014.
- Kahn, B. H., Schreier, M. M., Yue, Q., et al., *Pixel-scale assessment and uncertainty analysis of AIRS and MODIS ice cloud optical thickness and effective radius*, Journal of Geophysical Research: Atmospheres, 120(22), pp. 11,669-11,689, 2015.
- King M.D., *Determination of the Scaled Optical Thickness of Clouds from Reflected Solar Radiation Measurements*, Journal of the Atmospheric Sciences, 44(13), pp. 1734-1751, 1987.

- King M.D., Kaufman Y.J., Menzel W.P., Tanre D., *Remote sensing of cloud, aerosol, and water vapor properties from the moderate resolution imaging spectrometer (MODIS)*, IEEE Transactions on Geoscience and Remote Sensing, 30, pp. 2-27, 1992.
- King, M. D., Menzel, W. P., Kaufman, Y. J., et al., *Cloud and aerosol properties, precipitable water, and profiles of temperature and water vapor from MODIS*, IEEE Transactions on Geoscience and Remote Sensing, 41(2), pp. 442-458, 2003.
- Krisna, T. C., Wendisch, M., Ehrlich, A., et al., *Comparing airborne and satellite retrievals of cloud optical thickness and particle effective radius using a spectral radiance ratio technique: two case studies for cirrus and deep convective clouds*, Atmospheric Chemistry and Physics, 18(7), pp. 4439-4462, 2018.
- Li, J., Huang, H. L., Liu, C. Y., et al., *Retrieval of cloud microphysical properties from MODIS and AIRS*, Journal of Applied Meteorology, 44(10), pp. 1526-1543, 2005.
- Li, J., Zhang, F., Li, W., et al., *Transfer-learning-based approach to retrieve the cloud properties using diverse remote sensing datasets*, IEEE Transactions on Geoscience and Remote Sensing, 61, pp. 1-10, 2023.
- Ling F., Lu Z., Luo J. J., Bai L., Behera S. K., Jin D., Pan B., Jiang H., and Yamagata T., *Diffusion Model-based Probabilistic Downscaling for 180-year East Asian Climate Reconstruction*, 2024, arXiv preprint arXiv:2402.06646.
- Li, L., Carver, R., Lopez-Gomez, I., et al., *Generative emulation of weather forecast ensembles with diffusion models*, Science Advances, 10(13), eadk4489, 2024.
- Meng X., Cheng J., Guo H., Yao B., *Quality Assessment of FY-4A/AGRI Official Sea Surface Temperature Product*, IEEE Geoscience and Remote Sensing Letters, 21, pp. 1-5, 2024.
- Menzel, W. P., Frey, R. A., Zhang, H., et al., *MODIS Global Cloud-Top Pressure and Amount Estimation: Algorithm Description and Results*, Journal of Applied Meteorology and Climatology, 47(4), pp. 1175-1198, 2008.
- Min M., Li J., Wang F., Liu Z., Menzel W.P., *Retrieval of cloud top properties from advanced geostationary satellite imager measurements based on machine learning algorithms*, Remote Sensing of Environment, 239, pp. 111616, 2020.
- Muskatel H.B., Blahak U., Khain P., Levi Y., Fu Q., *Parametrizations of liquid and ice clouds' optical properties in operational numerical weather prediction models*, Atmosphere, 12(1), pp. 89, 2021.

- Nai C., Pan B., Chen X., Tang Q., Ni G., Duan Q., Lu B., Xiao Z., and Liu X., *Reliable precipitation nowcasting using probabilistic diffusion models*, Environmental Research Letters, 19, pp. 034039, 2024.
- Nauss T., Kokhanovsky A.A., *Retrieval of warm cloud optical properties using simple approximations*, Remote Sensing of Environment, 115(6), pp. 1317-1325, 2011.
- Pan B., Wang L. Y., Zhang F., Duan Q., Li X., Pan X., ..., & Xiao Z., *Probabilistic diffusion model for stochastic parameterization—a case example of numerical precipitation estimation*, 2023, Authorea Preprints.
- Parol F., Buriez J.C., Brogniez G., Fouquart Y., *Information Content of AVHRR Channels 4 and 5 with Respect to the Effective Radius of Cirrus Cloud Particles*, Journal of Applied Meteorology, 30(7), pp. 973-984, 1991.
- Platnick S., Valero F.P.J., *A validation of a satellite cloud retrieval during ASTEX*, Journal of the Atmospheric Sciences, 52(16), pp. 2985-3001, 1995.
- Platnick S. et al., *MODIS atmosphere L2 cloud product (06_L2)*, NASA MODIS Adaptive Processing System, Goddard Space Flight Center, 2015, DOI: 10.5067/MODIS/MOD06_L2.
- Platnick, S., King, M. D., Ackerman, S. A., et al., *The MODIS cloud products: algorithms and examples from Terra*, IEEE Transactions on Geoscience & Remote Sensing, 41(2), pp. 459-473, 2003.
- Platnick, S., Meyer, K. G., King, M. D., et al., *The MODIS cloud optical and microphysical products: Collection 6 updates and examples from Terra and Aqua*, IEEE Transactions on Geoscience & Remote Sensing, 55(1), pp. 502-525, 2016.
- Rodgers C.D., *Inverse Methods for Atmospheric Sounding (Theory and Practice) — Introduction*, World Scientific, pp. 1-11, 2000.
- Sohl-Dickstein J., Weiss E., Maheswaranathan N., Ganguli S., *Deep unsupervised learning using nonequilibrium thermodynamics*, International Conference on Machine Learning, PMLR 37, pp. 2256-2265, 2015.
- Song Y., Ermon S., *Generative modeling by estimating gradients of the data distribution*, Advances in Neural Information Processing Systems, 32, 2019.
- Song, Y., Sohl-Dickstein, J., Kingma, D.P., Kumar, A., Ermon, S., Poole, B., *Score-based generative modeling through stochastic differential equations*, International Conference on Learning Representations, 2021.
- Stephens, G. L., & Webster, P. J., *Clouds and Climate: Sensitivity of Simple Systems*, Journal of the Atmospheric Sciences, 38(2), pp. 235-247, 1981.

- Stephens G.L., Tsay S.C., P.W.S. Jr, Flatau P.J., *The Relevance of the Microphysical and Radiative Properties of Cirrus Clouds to Climate and Climatic Feedback*, Journal of the Atmospheric Sciences, 47(14), pp. 1742-1754, 1990.
- Tang G., Panetta R.L., Yang P., Kattawar G.W., Zhai P.-W., *Effects of ice crystal surface roughness and air bubble inclusions on cirrus cloud radiative properties from remote sensing perspective*, Journal of Quantitative Spectroscopy & Radiative Transfer, 195, pp. 119-131, 2017.
- Tong, X., Li, J., Zhang, F., et al., *The Deep-Learning-Based Fast Efficient Night-time Retrieval of Thermodynamic Phase From Himawari-8 AHI Measurements*, Geophysical Research Letters, 50(11), e2022GL100901, 2023.
- Toshiro I., *On the Temperature and Effective Emissivity Determination of Semi-Transparent Cirrus Clouds by Bi-Spectral Measurements in the 10 μ m Window Region*, Journal of the Meteorological Society of Japan, 63(1), pp. 88-99, 1985.
- Trebing K., Stańczyk T., & Mehrkanoon S., *SmaAt-UNet: Precipitation nowcasting using a small attention-UNet architecture*, Pattern Recognit Lett, 145, pp. 178–186, 2021, <https://doi.org/10.48550/arXiv.2007.04417>.
- Twomey S., T. Cocks, *Remote sensing of cloud parameters from spectral reflectance in the near-infrared*, Beiträge zur Physik der Atmosphäre, 62(3), pp. 172-179, 1989.
- Vaswani, A., Shazeer, N., Parmar, N., Uszkoreit, J., Jones, L., Gomez, A. N., ... & Polosukhin, I., *Attention is all you need*, Advances in neural information processing systems, 2017, 30.
- Waliser, D. E., Li, J. L. F., Woods, C. P., et al., *Cloud ice: A climate model challenge with signs and expectations of progress*, Journal of Geophysical Research: Atmospheres, 114(D8), D00A21, 2009.
- Wang C., S. Platnick, Z. Zhang, K. Meyer, P. Yang, *Retrieval of ice cloud properties using an optimal estimation algorithm and MODIS infrared observations: 1. Forward model, error analysis, and information content*, Journal of Geophysical Research: Atmospheres, 121(10), pp. 5809-5826, 2016a.
- Wang, C., Platnick, S., Zhang, Z., et al., *Retrieval of ice cloud properties using an optimal estimation algorithm and MODIS infrared observations: 2. Retrieval evaluation*, Journal of Geophysical Research: Atmospheres, 121(10), pp. 5827-5845, 2016b.
- Wang, Q., Zhou, C., Zhuge, X., et al., *Retrieval of cloud properties from thermal infrared radiometry using convolutional neural network*, Remote Sensing of Environment, 278, pp. 113079, 2022.

Zhang Z., S. Platnick, *An assessment of differences between cloud effective particle radius retrievals for marine water clouds from three MODIS spectral bands*, Journal of Geophysical Research: Atmospheres, 116(D20), pp. D20215, 2011.

Zhao, Z., Zhang, F., Wu, Q., et al., *Cloud Identification and Properties Retrieval of the Fengyun-4A Satellite Using a ResUNet Model*, IEEE Transactions on Geoscience and Remote Sensing, 61, pp. 1-18, 2023.

Zhuge X., X. Zou, Y. Wang, *AHI-Derived Daytime Cloud Optical/Microphysical Properties and Their Evaluations With the Collection-6.1 MOD06 Product*, IEEE Transactions on Geoscience and Remote Sensing, 59(8), pp. 6431-6450, 2020.